Heliyon 6 (2020) e04724

Contents lists available at ScienceDirect

Heliyon

journal homepage: www.cell.com/heliyon

Research article

PES, molecular structure, spectroscopic (FT-IR, FT-Raman), electronic (UV-Vis, HOMO-LUMO), quantum chemical and biological (docking) studies on a potent membrane permeable inhibitor: dibenzoxepine derivative

S. Sevvanthi [a,b], S. Muthu [a,c,*], M. Raja [d], S. Aayisha [e], S. Janani [f]

[a] Department of Physics, Arignar Anna Govt. Arts College, Cheyyar, 604407, Tamilnadu, India
[b] Thiruvalluvar University, Serkkadu, Vellore, 632 115, Tamilnadu, India
[c] Department of Physics, Puratchi Thalaivar Dr M.G.R Govt Arts and Science College, Uthiramerur, 603406, Tamilnadu, India
[d] Department of Physics, Govt Thirumagal Mills College, Gudiyattam, 632602, Vellore, Tamilnadu, India
[e] Department of Physics, Meenakshi College for Women, Chennai, 600024, Tamilnadu, India
[f] Department of Physics, Queen Mary's College, Chennai 600005, Tamilnadu, India

ARTICLE INFO

Keywords:
Analytical chemistry
Materials chemistry
Theoretical chemistry
DFT
FT-IR
FT-Raman
NBO
Fukui functions
Docking

ABSTRACT

The dibenzoxepines derivatives have found a broad application in biological and pharmaceutical fields as new prospective drugs. So, the molecule (3aS,12bS)-5-Chlor-2-methyl-2,3,3a,12b-tetrahydro-1H-dibenzo[2,3:6,7]oxepino[4,5-c]pyrrol has been characterized by DFT (Density Functional Theory) approach to predict the important properties of it. The minimum energy conformer has been found by PES (Potential Energy Surface) and then the structure is optimized. Further, the structure is characterized spectroscopically by FT-IR and FT-Raman techniques to know the functional group and chemically active atoms. The geometrical parameters, PED (Potential Energy Distribution) assignments have also been reported. The electronic properties of the title compound have been explained by UV-Vis and HOMO-LUMO analyses that describe the charge transfer between the atoms of the molecule. Molecular Electrostatic Potential (MEP), Electron Localization Function (ELF) and Localized Orbital Locator (LOL) have been depicted to know the chemically active regions. The electrophilic and nucleophilic regions have been shown by Fukui functions. The Non-Linear Optics (NLO) for non-linear optical effects and the Natural Bond Orbital (NBO) for charge delocalization were studied. To study the biological activity of the title compound, molecular docking has been performed which suggests that the title molecule may act as a membrane permeable inhibitor.

1. Introduction

(3aS,12bS)-5-Chlor-2-methyl-2,3,3a,12b-tetrahydro-1H-dibenzo [2,3:6,7]oxepino[4,5-c]pyrrol (5TDOP) is a dibenzoxepine derivative compound. It has two benzene rings that are attached with oxepino[4,5-c]pyrrole ring with electrophilic functional groups (C–O, N–C and C–Cl). Oxepin is a heterocycle derivative that is acted as tricyclic antidepressant. This contains oxygen and three double bonds with seven-membered ring structure. In addition, dibenzoxepines and pyrrole derivatives play an essential role in wide range of biological activities such as DNA binding, antimicrobial, antioxidant, enzyme/receptor interactions, antidepressant, bipolar disorder, plasma therapy etc. [1, 2, 3, 4, 5]. 5TDOP compound has heterocyclic intermediate substituent pyrrole which is widely used in pharmaceuticals [2], production of agrochemicals, synthesis of dyes, photographic chemicals etc. It has aromatic nature which is a main feature of organic compound. Usually it reacts with electrophiles. Miller et al [6] reported that 5TDOP is an antipsychotic drug that has the aforesaid substituents. Antipsychotic drugs (APDs) are used for the treatment of schizophrenia and are also commonly used in the treatment of bipolar disorder with psychotic symptoms that is referred to bipolar I disorder. Now a days, many of the people are affected by bipolar I mental disorder due to stress. 5TDOP is a drug for Schizophrenia and bipolar disorders. The diseases namely schizophrenia, bipolar disorders cause serious neuropsychiatric disorders along with substantial health

* Corresponding author.
E-mail address: mutgee@gmail.com (S. Muthu).

https://doi.org/10.1016/j.heliyon.2020.e04724
Received 19 May 2020; Received in revised form 11 July 2020; Accepted 11 August 2020

risks in patients [7,8]. 5TDOP drug is approved by FDA for schizophrenia acute treatment and for the acute treatment of manic related to bipolar I disorder.

Raghunath Reddy Anugu, Prathama S. Mainkar et al [9] presented the ireland-claisen rearrangement strategy for the synthesis of schizophrenia drug, (+)-asenapine. Vaishali M. Gambhire et al [10] reported the enhanced oral delivery with asenapine maleate that taking from the solid lipid nanoparticles (pharmacokinetic and brain distribution evaluations). The compound has biological and chemical importance. So, to characterize and to know the properties of the 5TDOP, the spectroscopy and quantum chemical calculations are considered since that is not reported in literature. In the present study, the experimental and the theoretical spectroscopic (FT-IR, FT-Raman and UV-Vis) characterizations for 5TDOP have been reported. Molecular geometry, vibrational frequencies, molecular surface analysis and chemical reactivities are calculated using density functional theory with B3LYP method with 6–311++G(d,p) basis set. The stability of molecule was studied by Potential Energy Scan analysis (PES). The electronic properties are found by UV-Vis and HOMO-LUMO analyses with their fundamental chemical parameters. The molecular reactivities of electrophilic and nucleophilic characters are calculated using Fukui function and MEP surface analyses. In addition, the biological activity of antipsychotic nature in bipolar disorders for 5TDOP has been explained by molecular docking (protein-ligand) analysis.

2. Experimental methods

The solid form of 5TDOP that has purity of 98% has been purchased from the Sigma Aldrich Company. This pure 5TDOP has been taken to do characterization namely FT-IR, FT-Raman and UV-Vis analysis. The FT-IR spectrum has been precisely recorded from the range 4000 to 400 cm^{-1} by Perkin Elmer FT-IR Spectrum instrument which has resolution of 1.0 cm^{-1}. The FT-Raman spectrum of 5TDOP has been recorded by using BRUCKER RFS 27 instrument with Nd: YAG Laser of 100 mW from the range 4000 to 100 cm^{-1} in which the resolution is maintained as 2 cm^{-1}. The UV-Vis absorption spectrum of 5TDOP has been obtained with the usage of DMSO solvent from 200 to 600 nm by the spectrometer of Perkin Elmer LAMBDA 950 UV. These characterizations have been carried out at the institute of Sophisticated Analytical Instruments Facility (SAIF), IIT (M), Chennai, India.

3. Computational methods

Generally, DFT and HF quantum computational methods are utilized to predict the quantum states in many electron systems that are available in the molecule. The second method not contains the detail electronic correlation details [11]. So, for the present study, DFT technique which is more accurate and reliable was used to characterize 5TDOP. Gaussian 09W program was used to predict DFT calculations on 5TDOP by B3LYP/6-311++G(d,p) set for the characterization of the structure, electronic, chemical, biological and other properties [12, 13, 14]. The geometric parameters namely bond lengths and bond angles were obtained and the structure of 5TDOP has been depicted by Gauss View 5.0 [15]. The fundamental modes of vibrations using vibrational spectral calculations are done by VEDA software for the small 5TDOP molecule [16]. The UV-Vis analysis has been explained by using the calculations through TD-DFT method of Gaussian 09W output. The unscaled spectral values are scaled by using scaling factor 0.961 scaling factor which gives better agreement with the experimental values. HOMO-LUMO and MEP analyses were depicted using Gauss View 5.0 to explain the 5TDOP [17]. Furthermore, Multiwfn software [18] was used to explain electronic and chemical properties by DOS, LOL and ELF. The property namely NLO was obtained by Gaussian 09W output. AUTODOCK 1.4.6 and PYMOL software were used for the docking between the selected proteins [19] and 5TDOP to explain the biological behaviour.

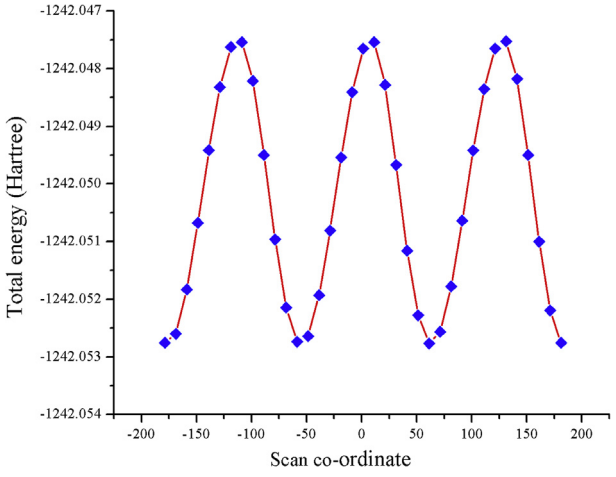

Figure 1. PES (Potential Energy Surface) graph of 5TDOP.

Table 1. Potential energy surface analysis of 5TDOP.

No. of Conformations	Scan coordinate (angle)	Total energy (hartree)
1	-178.7623	-1242.0528
2	-168.7623	-1242.0526
3	-158.7623	-1242.0518
4	-148.7623	-1242.0507
5	-138.7623	-1242.0494
6	-128.7623	-1242.0483
7	-118.7623	-1242.0476
8	-108.7623	-1242.0475
9	-98.7623	-1242.0482
10	-88.7623	-1242.0495
11	-78.7623	-1242.0510
12	-68.7623	-1242.0521
13	-58.7623	-1242.0527
14	-48.7623	-1242.0526
15	-38.7623	-1242.0519
16	-28.7623	-1242.0508
17	-18.7623	-1242.0495
18	-8.7623	-1242.0484
19	1.2377	-1242.0477
20	11.2377	-1242.0475
21	21.2377	-1242.0483
22	31.2377	-1242.0497
23	41.2377	-1242.0512
24	51.2377	-1242.0523
25	61.2377	-1242.0528
26	71.2377	-1242.0526
27	81.2377	-1242.0518
28	91.2377	-1242.0506
29	101.2377	-1242.0494
30	111.2377	-1242.0484
31	121.2377	-1242.0477
32	131.2377	-1242.0475
33	141.2377	-1242.0482
34	151.2377	-1242.0495
35	161.2377	-1242.0510
36	171.2377	-1242.0522
37	181.2377	-1242.0528

Table 2. Optimized geometrical parameters (bond length (Å) and bond angle (°)) of 5TDOP by 6–311++G(d,p) basis set.

Bond length(Å)			Bond angle(°)		
Bonds	B3LYP	Experimental*	Bonds	B3LYP	Experimental*
Cl1–C17	1.761	1.744	N3–C7–H26	110.0	-
O2–C11	1.385	1.209	N3–C10–H27	109.9	-
O2–C12	1.391	-	N3–C10–H28	112.9	-
N3–C6	1.458	1.458	N3–C10–H29	109.9	109.6
N3–C7	1.472	1.474	C5–C4–C6	101.4	-
N3–C10	1.449	1.463	C5–C4–C8	111.8	117.8
C4–C5	1.551	-	C5–C4–H21	108.3	108.5
C4–C6	1.526	-	C4–C5–C7	103.3	-
C4–C8	1.503	1.504	C4–C5–C9	116.3	116.8
C4–H21	1.096	-	C4–C5–H22	106.1	108.5
C5–C7	1.555	-	C6–C4–C8	119.1	119.4
C5–C9	1.517	1.514	C6–C4–H21	107.6	108.5
C5–H21	1.097	-	C4–C6–H23	113.3	116.5
C6–H23	1.094	-	C4–C6–H24	110.8	109.3
C6–H24	1.107	-	C8–C4–H21	108.2	108.5
C7–H25	1.102	-	C4–C8–C11	117.1	117.6
C7–H26	1.094	-	C4–C8–C13	124.6	121.8
C8–C11	1.399	1.388	C7–C5–C9	115.8	118.6
C8–C13	1.396	1.388	C7–C5–H22	107.4	-
C9–C12	1.405	1.403	C5–C7–H25	110.2	-
C9–C14	1.404	1.400	C5–C7–H26	112.2	-
C10–H27	1.093	-	C9–C5–H22	107.3	-
C10–H28	1.107	-	C5–C9–C12	124.4	125.3
C10–H29	1.093	-	C5–C9–C14	118.9	118.8
C11–C15	1.390	-	H23–C6–H24	107.9	107.9
C12–C16	1.397	-	H25–C7–H26	107.5	107.5
C13–C17	1.392	-	C11–C8–C13	118.3	-
C13–H30	1.082	-	C8–C11–C13	121.5	121.9
C14–C18	1.390	-	C8–C11–C17	120.1	-
C14–H31	1.084	-	C8–C13–H30	120.5	-
C15–C19	1.393	-	C12–C9–C14	116.7	117.8
C15–C19	1.083	0.930	C9–C12–C16	121.1	-
C16–C20	1.388	1.380	C9–C14–C18	122.6	-
C16–H33	1.083	0.930	C9–C14–H31	118.5	119.0
C17–C19	1.389	1.385	H27–C10–H28	108.2	-
C18–C20	1.393	-	H27–C10–H29	107.7	-
C18–C34	1.084	0.970	H28–C10–H29	108.0	-
C19–H35	1.082	0.960	C11–C15–C19	120.0	-
C20–H36	1.084	0.970	C11–C15–H32	119.2	-
Bond angle(°)			C12–H16–C20	120.7	-
Cl1–C17–C13	119.1	117.3	C12–C16–H33	117.9	-
Cl1–C17–C19	119.5	119.7	C17–C13–H30	119.4	-
C11–O2–C12	122.8	121.9	C13–C17–C19	121.4	-
O2–C11–C8	120.6	120.4	C18–C14–H31	118.9	-
O2–C11–C15	117.7	-	C14–C18–C20	119.4	-
C2–C12–C9	125.1	125.3	C14–C18–H34	120.0	-
C2–C12–C16	113.7		C19–C15–H32	120.8	-
C6–N3–C7	108.1	109.5	C15–H19–C17	118.8	-
C6–N3–C10	115.6	111.8	C15–C19–H35	120.8	-
N3–C6–C4	102.0	-	C20–H16–H33	121.4	-
N3–C6–H23	110.7	109.5	C16–C20–C18	119.4	-
N3–C6–H24	112.2	109.5	C16–C20–H36	119.9	-
C7–N3–C10	115.1	110.5	C17–C19–H35	120.5	-
N3–C7–C5	105.4	-	C20–C18–H34	120.6	-
N3–C7–H25	111.6	109.6	C18–C20–H36	120.7	-

* Taken from Ref [9].

4. Results and discussion

4.1. Geometrical parameters

The molecule 5TDOP has a molecular formula $C_{17}H_{16}ClNO$ with a molecular weight of 285.768 g/mol. Potential Energy Scan analysis (PES) is most successful approach for finding the molecular stability through conformation analysis [20]. The stability of 5TDOP is analyzed by PES using HF/6-31G(d,p) basis set which is given in Figure 1. PES has been processed and 37 energy conformers have been obtained with the rotation angles to predict stable structure. In Figure 1, blue dots represent the 37 energy conformer and 37 conformations are tabulated in Table 1. The total energy has been obtained as -1242.0527 Hartree with the angle of 183.62°. This minimum energy conformer of 5TDOP has been taken for the further characterization to predict the structural, electronic, chemical, biological properties of the molecule.

Geometrical parameters play most significant role in theoretical investigations on organic compounds because; it is found the stability of the molecules [17,20]. The optimized geometrical parameters of 5TDOP is calculated by density functional theory with the help of B3LYP methods and 6-311++G(d,p) set of functions. At present, many of the researchers reported B3LYP/6-311++G(d,p) method of geometrical parameter calculations on many compounds that are in very good agreement with the experimental ones. In the present study, the geometrical parameters in terms of bond length and bond angles are calculated and the values are reported in Table 2. 5TDOP possesses various types of bond lengths (C–C, C–Cl, C–H, C–N, and C–O) in which two major part of benzene rings R_1, R_2 and oxepino [4,5-c]pyrrole rings are present. The optimized molecular structure along with bond lengths and bond angles is shown in Figure 2.

Oxepino [4,5-c]pyrrole ring has higher C–C bond lengths compare to benzene rings R_1, R_2. The pyrrole ring C–C bond lengths are calculated at C5–C7/1.555, C5–C4/1.551, C4–C6/1.526, C5–C9/1.517, C4–C8/1.503Å and benzene rings C–C bond lengths varying from 1.388 to 1.405 Å. The Oxepino and benzene ring R_1 are attached with C=C bond with higher bond length value C9–C12/1.405Å and benzene ring R_1 C=C bond lengths are gradually decreased (C14–C18/1.390, C20–C16/1.388 Å). The C=C and C–C bond lengths of benzene ring R_2 are lower than benzene R_1 and the differences are clearly visualized in Figure 2. The benzene ring R_2 has substitution of Cl atom that changes the nature of the benzene. The longest bond length is presented between C–Cl bond at 1.761Å and shortest bonds are between C–H bonds (1.082–1.084 Å) for 5TDOP molecule. So, 5TDOP bond length values can be increased and decreased because, pyrrole ring and Cl substitutions affects the surrounding bonds (ring R_1 and R_2).

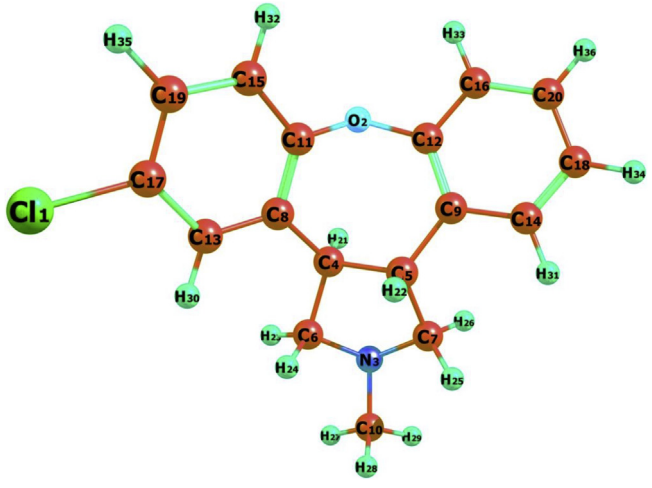

Figure 2. Optimized structure of 5TDOP using B3LYP/6-311++G(d,p) basis set.

4.2. Vibrational spectral analysis

The vibrational spectroscopy (FT-IR and FT-Raman) is efficient tool for structural conformational analysis of organic molecules [21]. 5TDOP consists 26 atoms with 86 normal modes of vibrations since it has non-linear molecular structure. It has 2 benzene rings, one methyl and two methylene group in it. The atoms oxygen, nitrogen and chlorine play an important role in structural elucidation. The experimental FT-IR and FT-Raman were recorded and theoretical vibrational frequency, IR and Raman intensities are calculated using 6-311++G(d,p) basis set and the values are listed in Table 3. Each vibrational mode with Potential Energy Distributions (PED) has been calculated using Veda 4 program. Figures 3 and 4 shows the comparative experimental and theoretical FT-IR and FT-Raman spectra and the correlation graph of Figure 5a, b represents the FTIR and FT-Raman. The scaled values of 5TDOP have been obtained from unscaled values after multiplying with the scaling factor 0.961 [22]. These scaled values are in agreement with the observed values that are reported in Table 3.

4.2.1. C–H vibrations

The aromatic, heterocyclic asymmetric and symmetric stretching C–H vibrations were found in the region of wave numbers 3000-2800 cm^{-1} [23,24]. In the current study, C–H stretching vibrations were observed at 3081 to 2778 cm^{-1} by B3LYP/6-311++G(d,p) basis set. The corresponding experimental FT-IR bands were observed at 2939(m), 2914(m) and the FT-Raman spectrum bands at 3075(w), 3047(w), 2965(s), 2947(s), 2911(s), 2774(w) at with the highest PED contribution value as 100% respectively. Similarly, the bending or bond deformation modes of vibrations appeared in the region between 1500 and 1300 cm^{-1} [25]. The theoretical frequencies were found to be in 1458, 1432 cm^{-1} which has close agreement with recorded FT-IR spectrum bands at 1461, 1424 cm^{-1} and with the strong intensity FT-Raman bands at 1458 cm^{-1} with 55 and 83 % of PED values. In general, in-plane bending of C–C–H vibrations are present as a number of strong to weak intensity bands in the region of 1300–1000 cm^{-1} [26]. The in plane bending vibrations for 5TDOP have been noted experimentally in FT-Raman spectrum as 1320, 1232, 1127 cm^{-1}. These values have good agreement with theoretical results that are obtained at 62, 45, 68% PED values. The H–C–H bending vibrations of 5TDOP have been observed at 1461(s) and 1424(s) cm^{-1} in FT-IR spectrum with theoretical values at 1458 and 1432 cm^{-1} with the PED values of 55 and 83%. The H–C–H bending vibration of 5TDOP has been observed at 1458(s) cm^{-1} in FT-Raman spectrum with theoretical value at 1458 cm^{-1} with the PED value of 55%.

4.2.2. C–C vibrations

The stretching vibrations (C=C bond) are supposed to be in the region 1650–800 cm^{-1} [27, 28, 29, 30, 31]. The C=C vibrations of 5TDOP are presented at the benzene rings (two in number) region. The theoretical values of 5TDOP were obtained in the range of 1570, 1544, 1214, 1030, 1025 cm^{-1} by B3LYP/6–311++G(d,p) method. The recorded bands which are of different intensities were observed at 1577(m), 1538(m), 1019(s) in FT-IR spectrum. The FT-Raman bands were identified at 1212(m), 1034(s) cm^{-1}. It shows that the theoretical values are in good agreement with the experimental data. The ring C–C–C vibrations of 5TDOP have been observed at 565(w) and 474(s) cm^{-1} in FT-Raman spectrum with the corresponding theoretical values at 576 and 471 cm^{-1} with the PED values of 43 and 37%. The observed values of 5TDOP have agreement with the scaled values of theoretical values.

4.2.3. C–N and C–Cl vibrations

The atom N3 is shared with the carbon atoms C6, C7 and C10 through single bond. The atoms C6 and C7 are attached with the methylene groups such as C6–H23–H24 and C7–H25–H26. The atom C10 is attached with the methyl group such as C10–H27–H28–H29. Due to this reason, the stretching N–C vibrations [32] have been observed at 824(w) cm^{-1} in FT-Raman spectrum with the theoretical value of 835 cm^{-1} with

Table 3. Calculated vibrational frequencies (cm^{-1}) assignments of 5TDOP (Experimental, theoretical by B3LYP/6-311++G(d,p) set).

Mode no	Experimental wave number (cm^{-1})		Theoretical wave number(cm^{-1})		I_{IR}[c]	I_{Raman}		Assignments (PED)[a]
	FTIR	FT-RAMAN	Unscaled	Scaled[b]		Relative	Absolute[d]	
102	-	-	3206	3081	0	555	13	γCH(88)
101	-	-	3204	3079	1	50	1	γCH(90)
100	-	3075(w)	3197	3073	4	704	16	γCH(88)
99	-	-	3191	3067	1	129	3	γCH(96)
98	-	-	3188	3064	8	340	8	γCH(87)
97	-	3047(w)	3175	3051	4	251	6	γCH(86)
96	-	-	3165	3041	1	110	3	γCH(91)
95	-	2965(s)	3092	2971	10	258	6	γCH(100)
94	2939(m)	2947(s)	3057	2938	16	439	10	γCH(92)
93	-	-	3051	2932	18	385	9	γCH(95)
92	-	-	3039	2921	20	214	5	γCH(91)
91	2914(m)	2911(s)	3034	2916	1	67	2	γCH(94)
90	-	-	2999	2882	4	392	9	γCH(91)
89	-	-	2946	2831	33	393	9	γCH(95)
88	-	-	2904	2791	61	751	18	γCH(90)
87	-	2774(w)	2891	2778	25	153	4	γCH(92)
86	-	-	1646	1582	3	262	6	γCC(59)
85	1577(m)	-	1634	1570	1	494	12	γCC(55)
84	-	-	1612	1549	4	458	11	γCC(45)
83	1538(m)	-	1607	1544	1	92	2	γCC(51)
82	-	-	1530	1470	4	116	3	βHCH(81)
81	1461(s)	1458(s)	1517	1458	6	62	1	βHCH(55)
80	-	-	1515	1456	2	29	1	βHCH(72)
79	-	-	1507	1448	91	59	1	βHCC(16)
78	-	-	1501	1443	5	99	2	βHCH(76)+τHCCC(10)
77	1424(s)	-	1490	1432	9	137	3	βHCH(83)
76	-	1423(m)	1472	1415	23	14	0	βHCC(52)
75	-	-	1457	1400	1	60	1	βHCN(82)
74	-	1387(s)	1433	1377	13	32	1	γCC(23)+βHCC(11)
73	-	1358(s)	1404	1349	6	126	3	βHCC(50)
72	-	1320(m)	1384	1330	7	101	2	βHCC(62)
71	-	-	1362	1309	9	279	7	τHCCC(29)
70	-	1285(m)	1343	1290	2	108	3	βHCC(37)
69	1280(m)	-	1331	1279	1	192	4	βHCC(38)+γCC(23)
68	-	-	1321	1270	16	182	4	βHCC(16)+γCC(49)
67	1258(m)	1259(m)	1309	1258	3	56	1	γCC(32)
66	-	-	1305	1254	7	23	1	βHCC(45)
65	-	-	1289	1239	1	37	1	βHCC(44)
64	-	1232(m)	1279	1229	14	156	4	βHCC(45)
63	-	1212(m)	1263	1214	100	298	7	γCC(56)
62	1201(m)	-	1253	1204	28	158	4	γCC(19)+τHCCC(37)
61	-	-	1233	1185	9	349	8	γCC(36)+βHCC(14)
60	-	-	1231	1183	4	140	3	βHCN(69)
59	-	-	1219	1172	11	1004	24	γCC(42)
58	-	-	1211	1163	43	49	1	γCC(30)
57	-	-	1196	1150	2	44	1	βHCC(37)
56	-	-	1186	1139	14	82	2	βHCC(27)
55	-	1127(vs)	1181	1135	2	98	2	βHCC(68)
54	-	-	1149	1105	6	151	4	βHCN(18)
53	1082(s)	1083(m)	1131	1087	10	40	1	βHCN(51)
52	-	-	1128	1084	7	64	1	βHCC(44)
51	-	-	1103	1060	18	536	13	βHCC(38)
50	-	-	1091	1048	7	71	2	γCC(40)
49	-	1034(s)	1072	1030	6	37	1	γCC(28)
48	1019(s)	-	1066	1025	0	816	19	γCC(51)
47	-	-	1051	1010	2	430	10	γCC(23)+τHCCC(19)
46	-	-	1043	1002	4	70	2	γCC(37)+τHCCC(11)

(*continued on next page*)

Table 3 (*continued*)

Mode no	Experimental wave number (cm^{-1})		Theoretical wave number(cm^{-1})		I_{IR}[c]	I_{Raman}		Assignments (PED)[a]
	FTIR	FT-RAMAN	Unscaled	Scaled[b]		Relative	Absolute[d]	
45	952(m)	-	988	949	0	3	0	τHCCH(89)
44	-	934(m)	984	945	0	29	1	γCC(10)+τHCCC(23)
43	929(m)	-	961	923	1	6	0	τHCCC(78)
42	-	-	958	921	1	40	1	τHCCC(76)+βHCC(10)+γCC(11)
41	-	-	958	920	10	6	0	γCC(11)+γCC(15)
40	879(s)	876(vs)	922	886	2	153	4	βHCC(43)
39	-	-	894	859	4	39	1	βHCC(10)+τHCNC(35)
38	-	-	877	843	4	43	1	γNC(15)+τHCCCl(56)
37	-	-	875	841	7	142	3	γNC(14)+τHCCCl(11)
36	-	824(w)	869	835	8	146	3	γNC(61)
35	-	-	846	813	11	13	0	γCC(11)+τHCCC(46)
34	-	783(m)	820	788	2	51	1	γCC(23)+τHCCC(15)
33	-	749(m)	775	745	9	25	1	βHCC(15)+τHCCC(11)
32	-	-	767	737	19	211	5	τHCCC(48)
31	-	713(w)	758	729	7	148	3	τHCCC(64)
30	704(s)	-	721	692	1	759	18	γCC(22)+τHCNC(16)+τHCCC(13)
29	-	648(m)	675	648	8	101	2	γClC(43)
28	630(s)	-	654	629	0	180	4	βHCC(47)
27	-	-	638	613	2	91	2	βHCC(50)
26	-	-	621	597	1	62	1	βHCC(49)
25	-	565(w)	599	576	4	86	2	βCCC(43)
24	588(s)	-	580	558	1	129	3	βHCC(15)+τHCCC(19)
23	-	517(m)	552	530	0	72	2	βHCC(10)+τHCCC(34)
22	-	-	518	498	2	88	2	τHCNC(40)
21	-	474(s)	490	471	2	127	3	βCCC(37)
20	-	-	475	456	4	123	3	τHCCC(12)+γClC(18)
19	-	417(w)	442	425	1	81	2	τHCCC(53)
18	-	-	410	394	1	244	6	τHCNC(35)+τHCNC(10)
17	-	367(m)	392	377	2	73	2	τHCCCl(36)
16	-	343(m)	368	354	0	124	3	τHCNC(30)
15	-	-	342	328	1	770	18	βHCC(21)
14	-	-	331	319	0	180	4	τHCNC(26)
13	-	-	324	312	2	1026	24	τHCNC(48)
12	-	289(m)	289	278	0	280	7	τHCNC(27)+βHCC(10)
11	-	-	275	264	2	356	8	βHCC(23)
10	-	243(m)	247	237	0	250	6	τHCNC(65)
9	-	-	236	227	0	886	21	τHCNC(40)
8	-	195(m)	209	201	0	608	14	τHCCC(26)
7	-	-	170	163	0	267	6	τHCCC(42)
6	-	127(s)	147	142	0	1331	31	τHCNC(13)
5	-	-	113	109	0	4267	100	τHCCC(57)
4	-	-	97	93	0	2487	58	τHCCC(68)
3	-	-	77	74	0	3696	87	τHCCC(62)
2	-	-	58	56	0	4022	94	τHCCC(57)
1	-	-	36	35	0	4150	97	βCOC(28)+τHCNC(14)

[a] γ-stretching,γ_a-Symmetrical stretching,γ_{as}-asymmetrical stretching, β-inplane bending,ω-outplane bending, τ-torsion, vs-very strong, s-strong, m-medium, w-weak.
[b] Scaling factor: 0.961 for B3LYP/6-311+G(d,p).
[c] Relative absorption intensities normalized with highest peak absorption equal to 100.
[d] Relative Raman intensities normalized to 100.

the PED value of 61%. The stretching mode of C–Cl vibrations is generally obtained in the region 760–505 cm^{-1} [33]. The atom Cl1 is attached with the carbon atom C17. The Cl1–C17 stretching vibration has been observed in FT-Raman spectrum as 648(m) cm^{-1} with the theoretical value as 648 cm^{-1} with 43% of PED.

4.2.4. Other vibrations

The bending H–C–N vibration is observed at 1082(s) cm^{-1} in FT-IR spectrum and 1083(m) cm^{-1} in FT-Raman spectrum with the corresponding theoretical value of 1087 cm^{-1} along with 51% of PED. The torsion H–C–C–C vibrations of 5TDOP have been measured at 1201(m) and 588(s) cm^{-1} in FT-IR spectrum with the theoretical values at 1204 and 558 cm^{-1}. The torsion H–C–C–C vibrations of 5TDOP have been measured at 934(m), 783(m), 749(m), 713(w), 517(m), 417(w) and 195(m) cm^{-1} in FT-Raman spectrum with the theoretical values at 945, 788, 745, 729, 530, 425 and 201 cm^{-1}. The torsion H–C–N–C vibration of 5TDOP has been measured at 704(s) cm^{-1} in FT-IR spectrum with the theoretical value at 692 cm^{-1}. The torsion H–C–N–C vibrations of 5TDOP

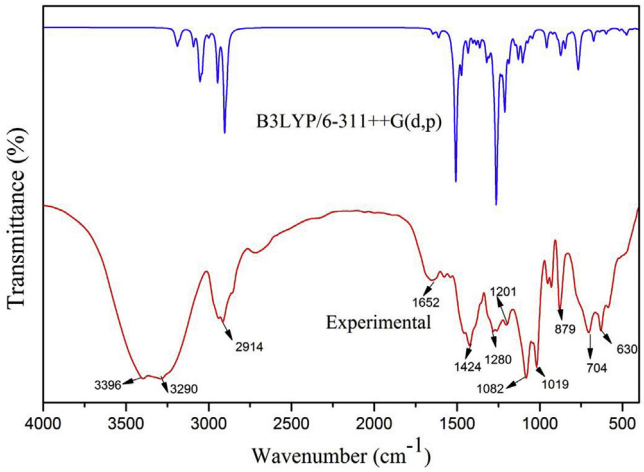

Figure 3. Experimental and theoretical FT-IR spectrum of 5TDOP.

has been measured at 343(m), 289(m), 243(m) and 127(s) cm^{-1} in FT-Raman spectrum with the theoretical values at 354, 278, 237, 142 cm^{-1}. The other theoretical H–C–C–C, H–C–N–C and H–C–C–Cl torsion vibrations have been reported in Table 3. Thus the vibration wavenumbers were estimated in theoretical approach has been favorable agreement with the recorded FT-IR and FT-Raman values.

4.3. Electronic properties

The experimental UV-Vis spectrum of 5TDOP has been performed in DMSO solution and the theoretical UV-Vis spectrum has been computed using TD-DFT/6-311++G(d,p) basis set by employing the same DMSO as a solvent. The results of both experimentally and theoretically (TD-DFT) calculated absorption wavelength (λ), excitation energies (E) and oscillator strengths (f) are the major factors during the electronic transitions and these are depicted in Table 4. As shown in Figure 6 the theoretical absorption values at 239, 236, 220 nm are associated with the 0.0412, 0.0216, 0.0328 oscillator frequencies and its major contributions are HOMO-1->LUMO (34%), HOMO-2->LUMO (18%), HOMO->LUMO (27%), HOMO->LUMO+1 (23%) along with the experimental value at 245 nm. The energy gap (ΔE) values of 5TDOP have found to be 5.2014 (H-1->LUMO (34%)), 5.2675 (H-2->LUMO (18%)), 5.6506 eV (HOMO->LUMO (27%)) with the corresponding experimental value 5.0740 eV. Thus, the simulated UV-Vis spectrum and experimental peaks are in good agreement with each other.

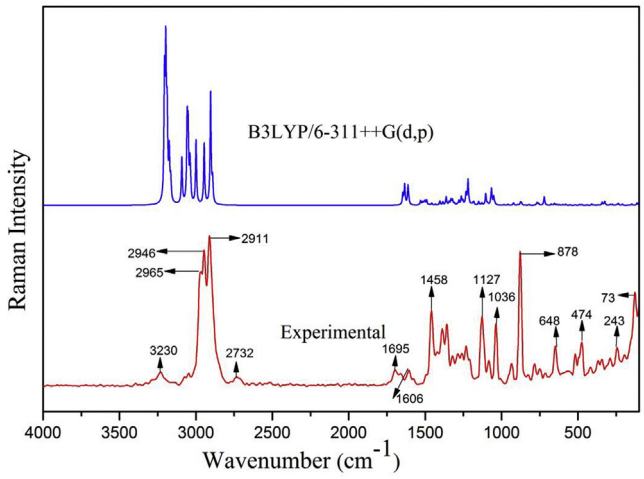

Figure 4. Experimental and theoretical FT-Raman spectrum of 5TDOP.

FMOs play an important role during molecular interactions. Further, the energy difference between the molecular orbitals provides a significant perspective about the optical, electronic properties and chemical reactivity of the molecule under investigation [34, 35, 36]. The HOMO (highest occupied molecular orbital) is the orbital which is signified as an electron donor (filled state) and therefore the LUMO (lowest unoccupied molecular orbital) symbolize the electron acceptor (empty state). The HOMO and LUMO energies and their orbital energy gap were computed using the B3LYP/6-311++G(d,p) technique. The simulated FMO's were depicted in Figure 7 in which a positive phase is shown in green and the negative is shown in red that represents the charge transfer within the molecule. The calculated band gap energy value Energy gap (eV) = 5.1084 eV of 5TDOP confirms the chemical stability of the molecule. Further, the HOMO (MO) and LUMO (MO) values are related to the ionization potential (electron-donating) and electron affinity (electron-accepting) of the compound. The Global molecular reactivity descriptors such as Electronegativity, Chemical hardness, Chemical softness (S), chemical potential (μ) and electrophilicity index (ω) electronic charge were predicted for 5TDOP and given in the Table 5. The parameters determined using the relation as,

$$\text{Chemical Potential} = 1/2\ (E_{LUMO} + E_{HOMO}) \quad (1)$$

$$\text{Electro negativity} = -1/2\ (E_{LUMO} + E_{HOMO}) \quad (2)$$

$$\text{Chemical hardness} = 1/2\ (E_{LUMO}\text{-}E_{HOMO}) \quad (3)$$

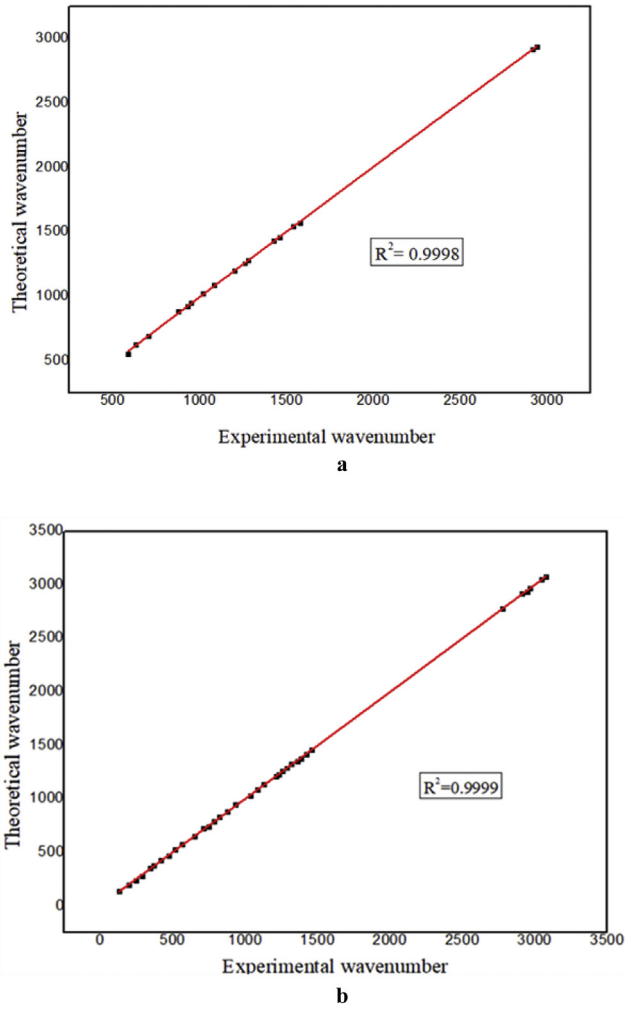

Figure 5. Correlation graph of (Fig. a represents the FT-IR and Fig. b represents the FT-Raman).

Table 4. UV-Vis absorption spectrum of 5TDOP (Experimental, Theoretical by B3LYP/6-311++G(d,p) set).

Experimental		TD-DFT/6-311++G(d,p)				
λ_{cal} (nm)	Band gap (eV)	λ_{cal} (nm)	Band gap (eV)	Energy (cm^{-1})	f	Assignment
245	5.0740	239	5.2014	41803	0.0412	H-4->L+2 (11%), H-1->LUMO (34%), H-1->L+2 (10%)
-	-	236	5.2675	42323	0.0216	H-2->LUMO (18%), H-1->L+2 (10%)
-	-	220	5.6506	45501	0.0328	HOMO->LUMO (27%), HOMO->L+1 (23%), HOMO->L+3 (16%)

$$\text{Electrophilicity index} = \mu^2/2\eta \quad (4)$$

$$\text{Chemical Softness} = 1/\eta \quad (5)$$

The 5TDOP has the ionization potential value (6.0448) which is much higher than the value of electron affinity (0.9364) that makes a finding of greater electron donor capability (ω-) of header compound as compared to electron acceptor capability (ω+) values. All these values may lead the biological activity of 5TDOP.

The Density of States graph of 5TDOP has been obtained by Multiwfn software to predict the electrical property [20] of the molecule. The band gap value that obtained in DOS is in agreement with the band gap values of UV-Vis analysis and HOMO-LUMO analysis. The small band gap of 5TDOP indicates the interaction between the atoms that are important in electronic and NLO property. Figure 8 represents the DOS diagram of 5TDOP in which black curve indicate total density of states, red curve indicate the density of states due to electronegative atoms (such as Cl, N and O atoms), blue curve depict the density of states due to carbon atoms, pink curve represents the density of states due to hydrogen atoms, green curve indicate the overlapping density of states of the molecule. The dotted long black line separates the HOMO and LUMO orbital which is called as band gap. The small vertical blue line indicates the HOMO (filled) orbitals of 5TDOP. The transmission from HOMO to LUMO has been shown clearly in Figure 8 that shows the charge transfer with in the molecule. The HOMO transitions are started from 0.22 a.u. (-0.22*27.211 = 5.986 eV). One of the LUMO transition values is noted as 0.05 a. u. (0.05*27.211 = 1.3 eV). Hence the DOS figure shows the HOMO-LUMO transitions for the molecule.

4.4. Natural Bond Orbital (NBO) analysis

Natural bond orbital analysis is a significant tool for investigating the inter and intra molecular interactions between the bonds of atoms [37, 38, 39]. The donor–acceptor interactions, bonding type, electron density and stabilization energy have been calculated on ASN molecule at DFT/B3LYP method with 6–311++G(d,p) basis set using second-order perturbation theory and an important donor-acceptor interaction values are listed in Table 6. The higher stabilization energy (E2) is involved in the enormous charge transfer of donor–acceptor interactions with in the molecular system. In the present study, the higher stabilization energy is calculated in LP(Cl), LP(O) and LP(N) donors that are interacted with the neighboring antibonding acceptors $\pi^*(C_{17}–C_{19})$, $\pi^*(C_9–C_{12})$, and $\pi(C_6–H_{24})$, with the energies of 13.26, 13.95, and 7.86 kcal/mol for 5TDOP. The NBO and MEP analysis results indicate that the maximum electrophilic potential atoms are donating the electrons to the surrounding acceptors.

4.5. Fukui analysis

The Fukui functions are widely used for molecular reactivity analysis such as electrophilic, nucleophilic and free radical attacks in a molecular system [40]. The individual atomic sites of 5TDOP is calculated using natural population analysis (NPA) with B3LYP/6-311++G(d,p) basis set. The Fukui functions are calculated from following equations

$$f^+(\vec{r}) = q_r(N+1) - q_r(N) \quad \text{for nucleophilic attack} \quad (6)$$

$$f^-(\vec{r}) = q_r(N) - q_r(N-1) \quad \text{for electrophilic attack} \quad (7)$$

$$f^0(\vec{r}) = (q_r(N+1) - q_r(N-1))/2 \quad \text{for radical attack} \quad (8)$$

In these equations, q_r is the atomic charge (evaluated from Natural population analysis, electrostatic derived charge, etc.) at the rth atomic site with the neutral (N), anionic (N+1), cationic (N-1) chemical species. The dual descriptor is the best view of nucleophilicity and electrophilicity characters. Recently, Morrel et al [41] calculated and reported the nucleophilic, nucleophilic characters of organic molecules using dual descriptor analysis by using the following equation.

$$\Delta f(\vec{r}) = f^+(\vec{r}) - f^-(\vec{r}) \quad (9)$$

In the present study, the Fukui functions and the dual descriptors are displayed in Figures 9 and 10. In the Figure 9, nucleophilic, electrophilic and radical attacks have been represented by red, blue and Green colours. The nucleophilic attacks have been found around Cl1, O2, N3 C11, C12, C17, C18 and C19 atoms for 5TDOP. The electrophilic attacks have been found around C5, C6, C7, C9, C10, C13, C14, C15, C16 and C20 atoms. The results for the positive and the negative regions have been reported in Table 7.

The Dual descriptor states that, if $\Delta f(\vec{r}) > 0$, then the location is prone to nucleophilic attack, if $\Delta f(\vec{r}) < 0$, then the location is prone to electrophilic attack [37,40]. The higher nucleophilicity has been calculated at a lone pair of nitrogen and oxygen atoms. The Figure 10 represents NPA atomic charges that predict the reactivity order for the nucleophilic case as N3 > O2 > C18 > Cl1 > C12 > C17 > C11 > 19 > C4 atoms, electrophilic case as C13 > C15 > C14 > Cl0 > C7 > C16 > C6 > C5 > C20 > C9 atoms and radical case as C8 atom. The nucleophilic attacks usually play major role in biochemistry field. Here, the donation of electrons with attraction (electrophilic) and partially electrophilic characters in surrounding atomic sites are reported. In the molecular reactivity analysis of the Fukui functions, the dual descriptor is very well with the results from the MEP analysis of the 5TDOP molecule.

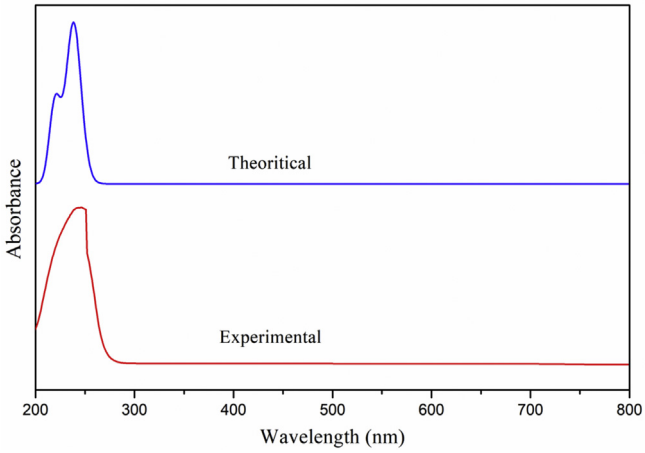

Figure 6. Experimental and theoretical UV-Vis absorption spectrum of 5TDOP.

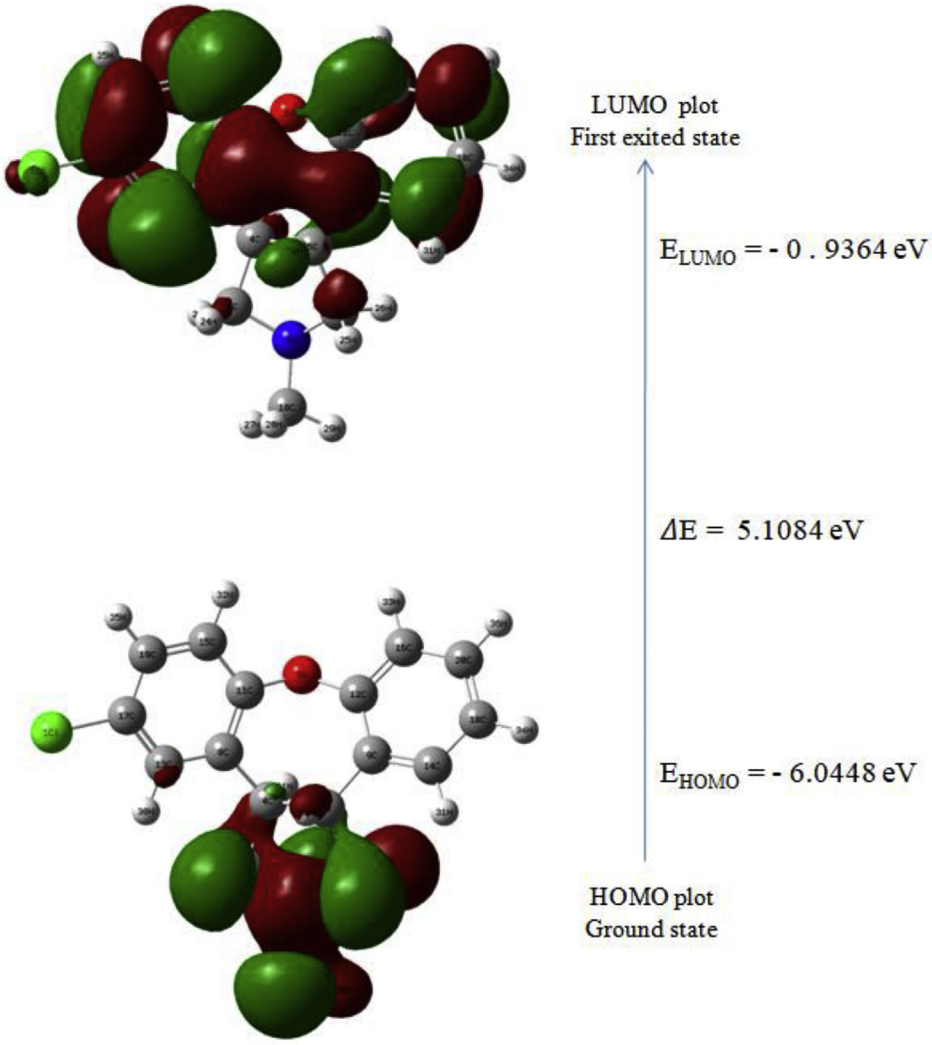

Figure 7. Frontier molecular orbital diagram (HOMO-LUMO) of 5TDOP with band gap values.

4.6. MEP, LOL, and ELF analysis

Molecular electrostatic potential surface analysis is the most successful approach to investigate electrophilic, nucleophilic and radical attack. It is very useful to analyze the molecular reactivity in organic, inorganic, polymer materials and also to identify the bio-molecular nature [42,43]. In the present study, the MEP surface of an ASN molecule is visualized by Gauss View 5.0 program and shown in Figure 11. In recent years, most of the researchers are used to visualize MEP surface using Gauss View 5.0 program in order to explain the different molecular electrostatic potential surfaces (in different colors for electrophilic, radial and nucleophilic attack that are presented by red, green and blue colors). The higher nucleophilic potential (Red color) is presented around N and O region in oxepino[4,5-c]pyrrole ring, partially nucleophilic (yellow colour) potential is presented around Cl and C atoms in Dibenzazepine (iminostilbene) ring and electrophilic potential is presented in C (pyrrole ring) and H atoms for 5TDOP molecule. The higher electrostatic potentials are concerned with an enormous amount of charge transfer during the intra and inter-molecular interactions in ASN molecule.

The Localized Orbital Locator (LOL) contributed by atoms [42] of 5TDOP has been explained through a color filled Plane map. LOL is one of the unique descriptors to know chemical bonding between the atoms of the molecule. The LOL plane map has been shown in Figure 12a and Figure 12b to know the chemically significant regions of 5TDOP. The benzene ring is shown by a blue color circle and BCP (Bond Critical Point) has been shown by red with yellow path at where delocalization of electrons of 5TDOP can be seen. Figure 12a represents the LOL due to electronegative atoms and Figure 12b represents the LOL due to whole atoms of the molecule.

Table 5. Calculated energy values of 5TDOP by B3LYP/6-311++G(d,p) by B3LYP/6-311++G(d,p) method.

Basis set	B3LYP/6-311+G(d,p)
HOMO(eV)	-6.0448
LUMO(eV)	-0.9364
Ionization potential	6.0448
Electron affinity	0.9364
Energy gap(eV)	5.1084
Electronegativity	3.4906
Chemical potential	-3.4906
Chemical hardness	2.5542
Chemical softness	0.1958
Electrophilicity index	2.3851
Electronic charge	1.3666
Electron donating capability (ω-)	4.4496
Electron accepting capability (ω+)	0.9591

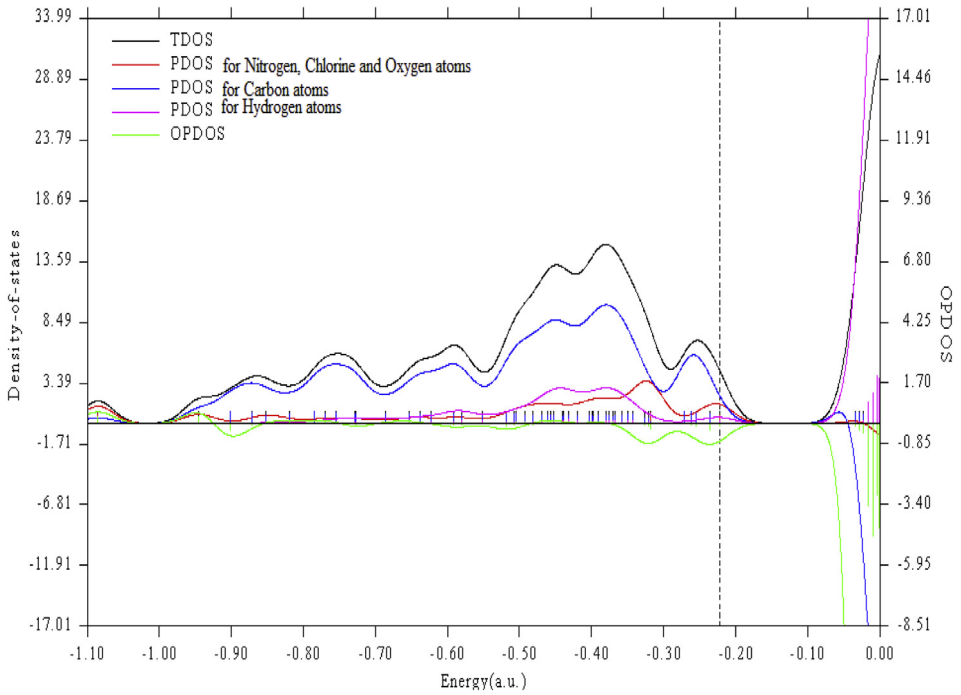

Figure 8. Density of States graph of 5TDOP with TDOS (Total Density of States), PDOS (Partial Density of States), OPDOS (Overlapping Density of states).

The Electron Localization Function (ELF) [45,20] of 5TDOP has been visualized Figure 13 with the Relief map which is a green map at the top of the topology image. Relief map shows the interactive interface of every atom in 5TDOP. Every atom is denoted by a peak (nuclei) with its electron distribution in the surroundings. The bottom map is ELF color filled map of 5TDOP. The BCP's, Chlorine, hydrogen, oxygen and carbon atoms have clearly shown in the figure with the electronic distribution. The lone pair at O and Cl atoms, electron depletion layer between inner and outer shell (blue circle around the nuclei) have also been shown in figure. Thus, these topology analyses suggest that the molecule 5TDOP is chemically active and hence it may possess biological applications.

Table 6. Second order perturbation theory analysis of Fock matrix in NBO basis for 5TDOP.

Donor(i)	ED/e	Acceptor(i)	ED/e	[a]E(2) (kJ mol^{-1})	[b]E(j)-E(i) (a.u.)	[c]F(i,j) (a.u.)
LP(1)Cl1	1.99124	π(C13–C17)	0.02877	1.87	1.48	0.047
		π(C17–C19)	0.02892	1.80	1.50	0.047
LP(2)Cl1	1.96892	π(C13–C17)	0.02877	4.59	0.87	0.056
		π(C17–C19)	0.02892	4.61	0.89	0.057
LP(3)Cl1	1.92449	π*(C17–C19)	0.40260	13.26	0.34	0.066
LP(1)O2	1.94950	π(C8–C11)	0.03625	5.77	1.04	0.069
		π(C9–C12)	0.03680	7.57	1.04	0.079
		π(C11–C15)	0.02557	1.12	1.04	0.031
		π*(C11–C15)	0.36148	1.84	0.50	0.030
		π(C12–C16)	0.02435	1.35	1.02	0.033
LP(2)O2	1.87009	π(C8–C11)	0.03625	1.34	0.95	0.033
		π*(C9–C12)	0.37986	13.95	0.43	0.074
		π(C11–C15)	0.02557	3.66	0.95	0.054
		π*(C11–C15)	0.36148	9.46	0.42	0.060
		π(C12–C16)	0.02435	1.51	0.93	0.034
LP(1)N3	1.88664	π(C6–H23)	0.01671	2.77	0.69	0.040
		π(C6–H24)	0.03457	7.86	0.66	0.066
		π(C7–H25)	0.02398	5.27	0.67	0.054
		π(C7–H26)	0.02033	4.31	0.69	0.050
		π(C10–H27)	0.00872	1.27	0.68	0.027
		π(C10–H28)	0.02639	8.24	0.67	0.068
		π(C10–H29)	0.00866	1.25	0.68	0.027

[a] $E^{(2)}$ means energy of hyper conjugative interaction (stabilization energy).
[b] Energy difference between donor and acceptor i and j NBO orbitals.
[c] F(i,j) is the Fock matrix element between i and j NBO orbitals.

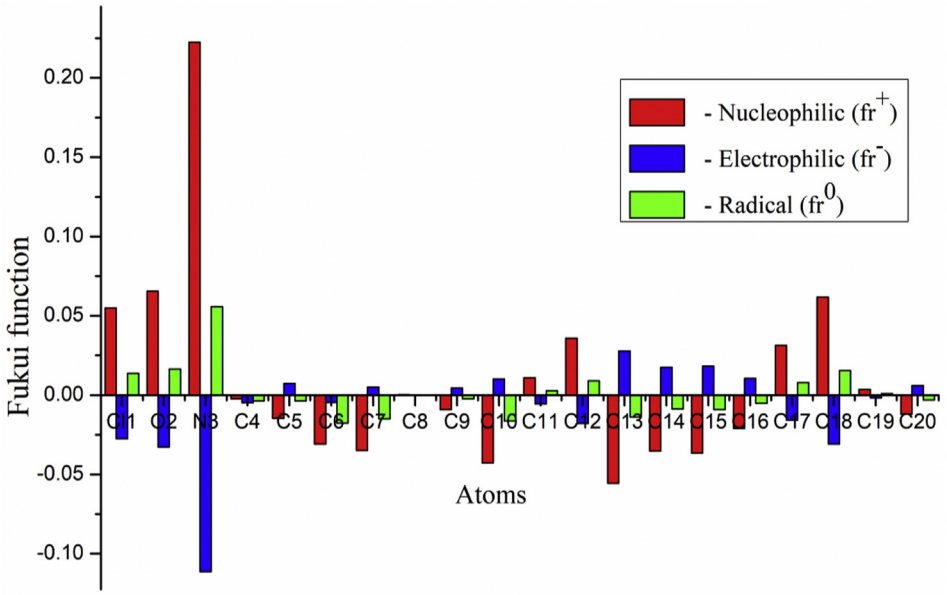

Figure 9. Fukui function graph for natural charges of 5TDOP.

4.7. NLO properties

Buckingham's definitions are usually used to calculate the NLO properties such as the dipole moment (μ), polarizability (α), and the first static hyperpolarizability (β) of the selected molecule through DFT calculations from Gaussian output [44]. The polarizability and the hyperpolarizability are the important tools in pharmacology, drug designing and in industrial fields as quantitative structure activity relationship tools [45]. The atoms that are in 5TDOP share its electrons unequally. Therefore, a difference in electronegativity creates dipole moment.

When the external electric field is weak and homogenous, this expansion becomes:

$$E = E^0 - \mu_\alpha F_\alpha - \tfrac{1}{2}(\alpha_{\alpha\beta}F_\alpha F_\beta) - \tfrac{1}{2}(\beta_{\alpha\beta\gamma}F_\alpha F_\beta F_\gamma) + \ldots \quad (10)$$

where E^0 is the energy of the unperturbed molecules, F_α the field at the origin μ_α, $\alpha_{\alpha\beta}$ and $\beta_{\alpha\beta\gamma}$ are the components of dipole moments, polarizability and the first hyperpolarizability [48-50]. The total static dipole moment μ, the mean polarizability α_0, the anisotropy of the polarizability Δα and the mean polarizability β_0, using the x,y,z components are defined as:

$$\mu = (\mu_x^2 + \mu_y^2 + \mu_z^2)^{1/2} \quad (11)$$

$$\alpha = (\alpha_{xx} + \alpha_{yy} + \alpha_{zz})/3 \quad (12)$$

$$\Delta\alpha = 2^{-1/2}[(\alpha^{xx} - \alpha^{yy})^2 + (\alpha^{yy} - \alpha^{zz})^2 + (\alpha^{zz} - \alpha^{xx})^2 + 6\alpha_{xx}^2]^{1/2} \quad (13)$$

$$\beta_0 = (\beta_x^2 + \beta_y^2 + \beta_z^2)^{1/2} \quad (14)$$

And

$$\beta_x = \beta_{xxx} + \beta_{xyy} + \beta_{xzz}$$
$$\beta_x = \beta_{yyy} + \beta_{yxx} + \beta_{yzz}$$
$$\beta_x = \beta_{zzz} + \beta_{zxx} + \beta_{zyy}$$

The dipole moment of the title molecule is 0.8516 which is a non-zero value that shows the larger value in electronegativity difference. The NLO parameters are shown in Table 8 in which the β value is compared to the reference NLO material urea. The β value of urea is 0.927×10^{-30} e.s.u and the β value of 5TDOP is $5.7285X10^{-30}$ e.s.u with the α of 3.2499×10^{-23} e.s.u. So, the title molecule may possess good NLO activity to produce second order non-linear effects. The polarizability of the molecule represents the changes in electron distribution. According to NBO analysis which is mentioned earlier, π- π* transactions indicate the intramolecular interaction that increases the polarizability value. The minimum band gap energy from HOMO-LUMO analysis also indicates the increase in NLO property of 5TDOP. Thus, 5TDOP may have electronic and biological significance.

4.8. Molecular docking analysis

The biological activities of title compound are estimated by molecular docking analysis. Molecular docking bioactive conformation is helpful for drug design with organic molecules. It is a preliminary analysis that reduces time and cost with simply identified protein-ligand energy interactions [46,47].

The 5TDOP molecule has the form of aminoimidazoles as BACE-1 Inhibitors. The aminoimidazoles as BACE-1 Inhibitors affect human beings and cause Alzheimer's disease. The Alzheimer's disease is a neurological disorder in which the death of brain cells causes memory loss and cognitive decline. Harald Hampel et al reported that BACE-1 Inhibitor is a most important drug target for slowing down Aβ (β-amyloid peptide) production in early Alzheimer's disease (AD). The BACE-1 inhibition has direct consequences in the Alzheimer's disease (AD) pathology without

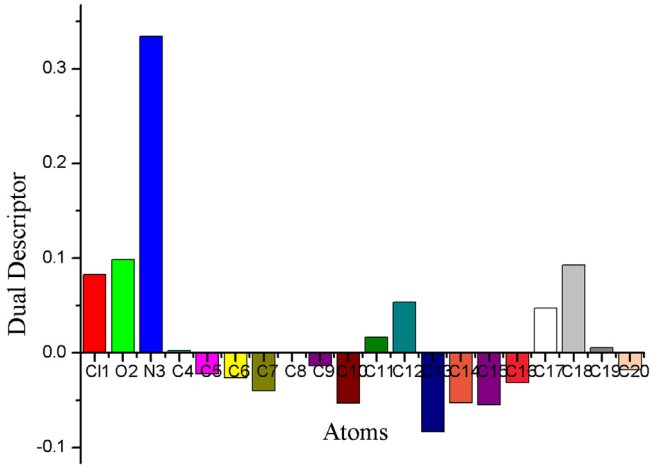

Figure 10. Fukui function graph for dual descriptor of 5TDOP.

Table 7. Fukui functions of 5TDOP with NPA atomic charges.

Atoms	Natural charges			Fukui functions			Dual descriptor (Δr)
	N	N +1	N-1	fr^+	fr^-	fr^0	
Cl1	0.0353	0.0903	0.0628	0.0550	-0.0275	0.0138	0.0825
O2	0.0057	0.0712	0.0384	0.0655	-0.0327	0.0164	0.0982
N3	0.0063	0.2289	0.1176	0.2226	-0.1113	0.0557	0.3339
C4	-0.0018	-0.0042	0.0030	-0.0024	-0.0048	-0.0036	0.0024
C5	0.0107	-0.0039	0.0034	-0.0146	0.0073	-0.0037	-0.0219
C6	0.0054	-0.0254	0.0100	-0.0308	-0.0046	-0.0177	-0.0262
C7	0.0112	-0.0237	0.0062	-0.0349	0.0050	-0.0150	-0.0399
C8	0.0023	0.0027	0.0025	0.0004	-0.0002	0.0001	0.0006
C9	0.0233	0.0142	0.0188	-0.0091	0.0045	-0.0023	-0.0136
C10	0.0158	-0.0270	0.0056	-0.0428	0.0102	-0.0163	-0.0530
C11	0.0085	0.0195	0.0140	0.0110	-0.0055	0.0028	0.0165
C12	-0.0062	0.0296	0.0117	0.0358	-0.0179	0.0090	0.0537
C13	0.0669	0.0115	0.0392	-0.0554	0.0277	-0.0139	-0.0831
C14	0.0359	0.0007	0.0183	-0.0352	0.0176	-0.0088	-0.0528
C15	0.0618	0.0252	0.0435	-0.0366	0.0183	-0.0092	-0.0549
C16	0.0459	0.0249	0.0354	-0.0210	0.0105	-0.0053	-0.0315
C17	0.0115	0.0428	0.0272	0.0313	-0.0157	0.0078	0.0470
C18	0.0112	0.0729	0.0421	0.0617	-0.0309	0.0154	0.0926
C19	0.0201	0.0236	0.0219	0.0035	-0.0018	0.0009	0.0053
C20	0.0371	0.0251	0.0311	-0.0120	0.0060	-0.0030	-0.0180

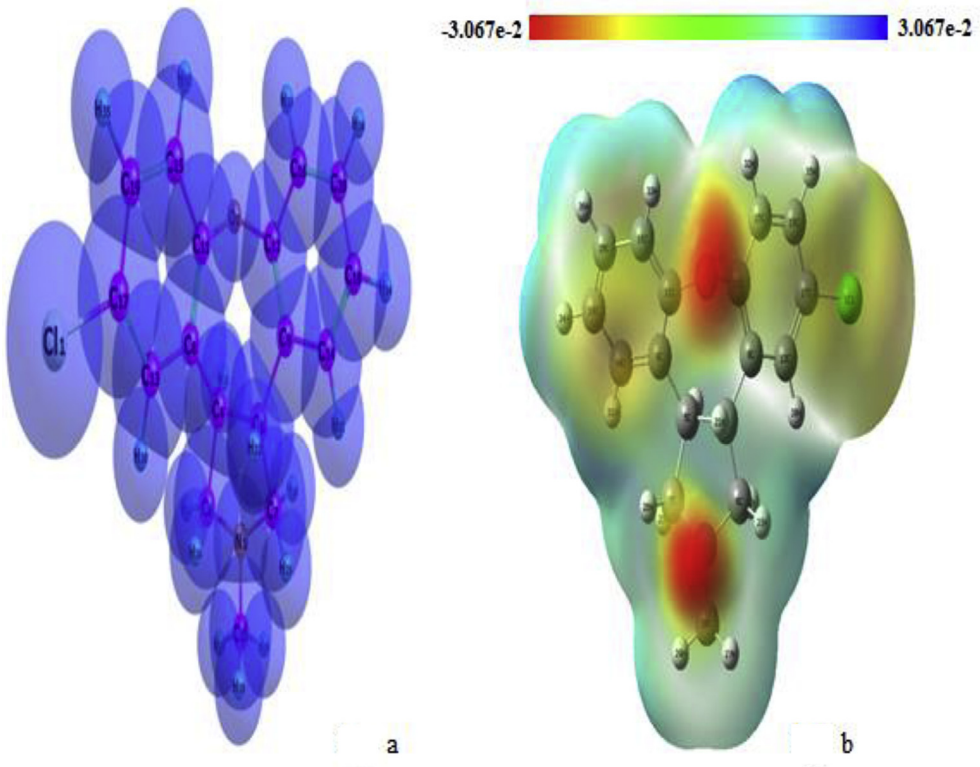

Figure 11. Molecular electrostatic potential diagram of 5TDOP (Fig. a represents the Van der Waals sphere for every atom, Fig. b represents the MEP surface).

largely affecting viability [1]. Thus, the activity of BACE-1 inhibition is satisfactory to interpreting schizophrenia like phenotypes [2]. Additional, chiriano et al [3] stated that the possible frameworks of amino-imidazole turned to be an validate its capability to interact with the BACE-1 inhibitor. Thus, the BACE-1 Inhibitors chosen with suitable protein targets such as 4B70, 4B72 are downloaded from the protein data bank. The protein-ligand interactions, binding energy, bond distance, estimate inhibition constant and RMSD values are calculated for the

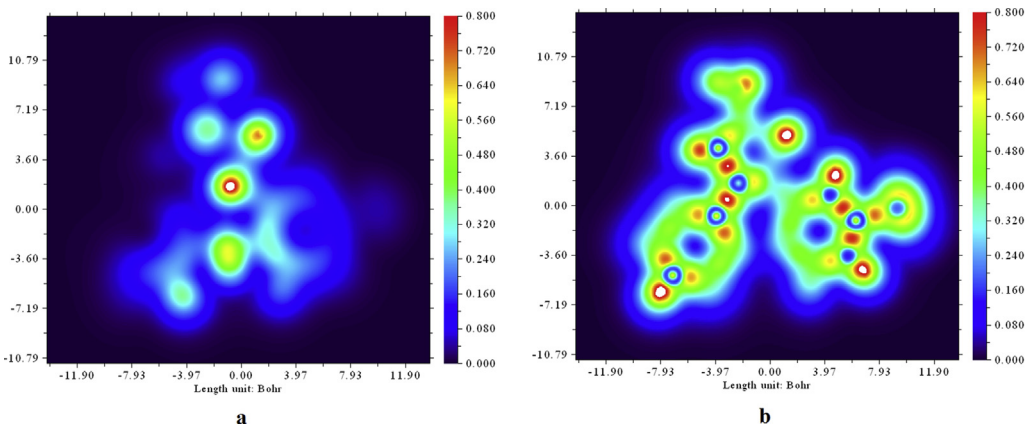

Figure 12. LOL (Localized orbital locator) of 5TDOP (Fig. a for electronegative atoms, Fig. b for whole molecule).

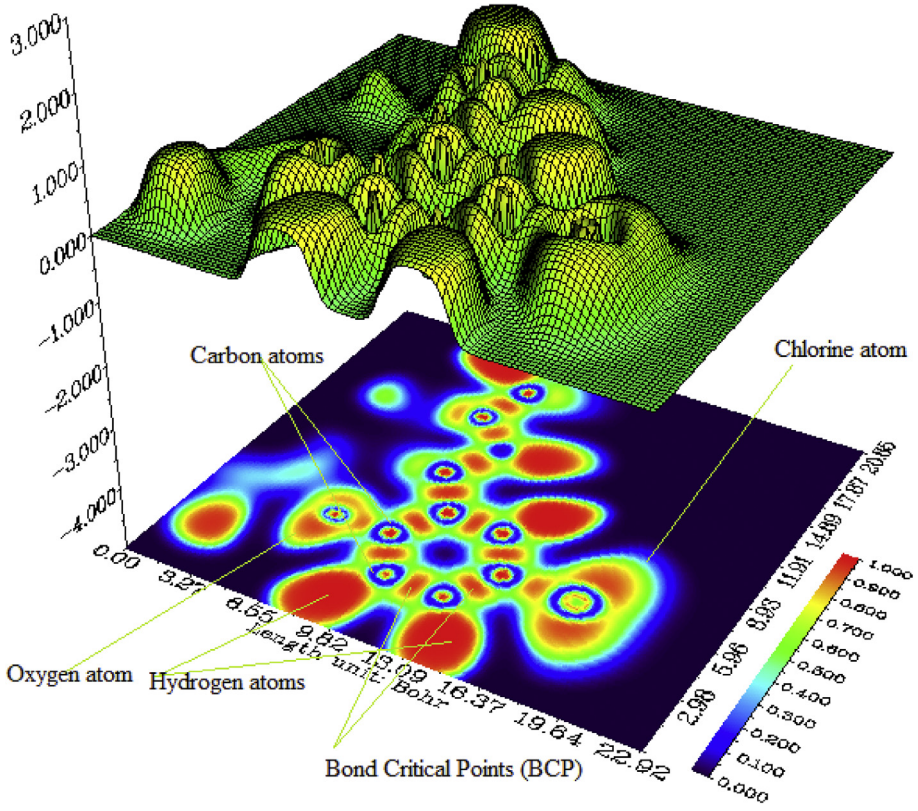

Figure 13. ELF (Electron localization function) with relief map of 5TDOP.

5TDOP molecule and the values have been listed in Table 9. The lowest binding energies have been observed as -6.31 kcal/mol with 4B70 protein and as -6.58 kcal/mol with 4B72 protein. The estimated inhibition constant has been calculated as 23.78 μm and 14.92 μm during the protein-ligand docking analysis. The lowest binding energies of the ligand 5TDOP molecule with the selected proteins are clearly illustrated in Figure 14 that the title molecule 5TDOP (antiaminoimidazoles) may inhibit BACE-1 and hence it may be a biologically significant molecule.

Table 8. The values of calculated dipole moment μ (D), polarizability (α_0), first order hyperpolarizability (βtot) components of 5TDOP.

Parameters	B3LYP/6-311++G(d,p)	Parameters	B3LYP/6-311++G(d,p)
μ_x	-0.57599	β_{xxx}	-400.17730
μ_y	-0.19195	β_{xxy}	-114.56300
μ_z	0.59710	β_{xyy}	9.24335
μ(D)	0.85160	β_{yyy}	-25.70450
α_{xx}	272.59830	β_{zxx}	135.45640
α_{xy}	8.42020	β_{xyz}	8.39180
α_{yy}	238.46580	β_{zyy}	102.77320
α_{xz}	2.61330	β_{xzz}	-65.19154
α_{yz}	-12.16064	β_{yzz}	36.23500
α_{zz}	146.81810	β_{zzz}	231.66410
α_0 (e.s.u)	3.2499×10^{-23}	βtot (e.s.u)	$5.7285X10^{-30}$
Δα(e.s.u)	$7.1938 x10^{-23}$		

Table 9. Molecular docking analysis of 5TDOP with proteins for membrane permeable inhibitor.

Protein (PDB ID)	Bonded residues	Bond distance (Å)	Estimated inhibition constant (μm)	Binding energy (kcal/mol)	Intermolecular energy (kcal/mol)	Reference RMSD (Å)
4B70	PHE′108	2.4	23.78	-6.31	-6.71	20.571
4B72		2.6	14.92	-6.58	-7.50	22.573

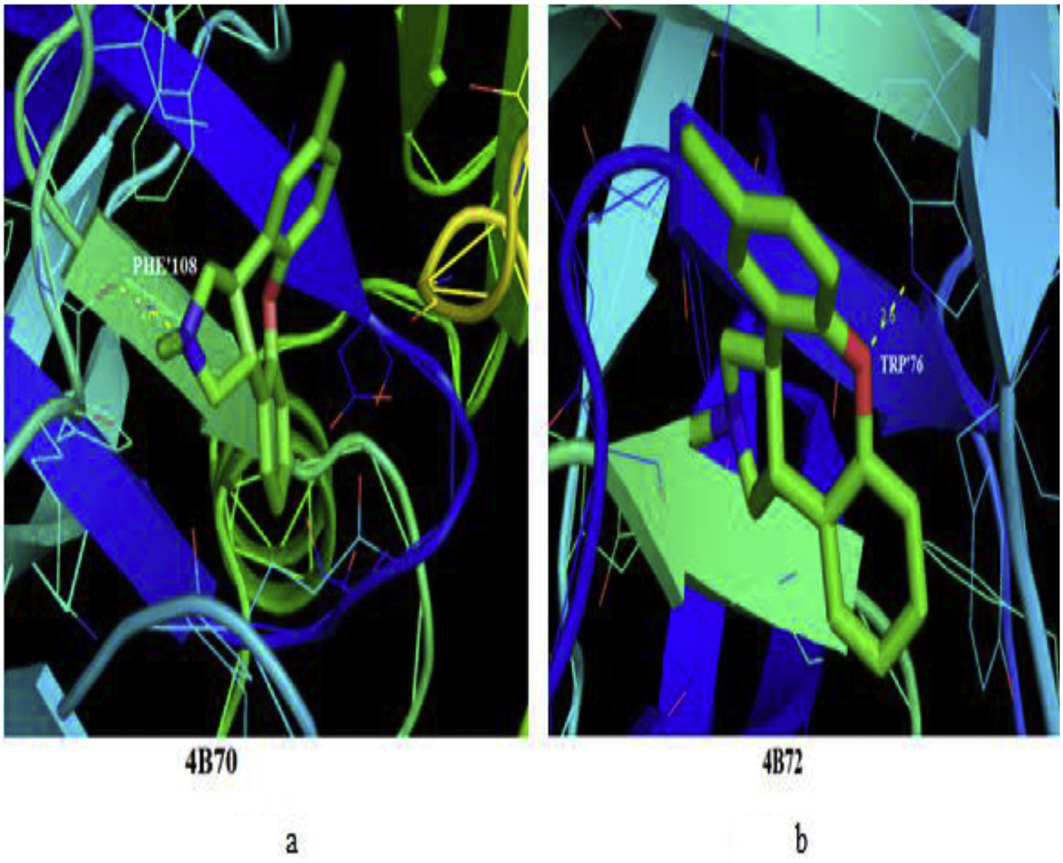

Figure 14. Molecular docking simulation of 5TDOP with the selected proteins (Fig. a for 4B70 and Fig. b for 4B72 proteins).

4.9. Conclusion

The aromatic, heterocyclic dibenzoxepine derivative molecule has been chosen. The molecular stability has been performed through PES conformation analysis. The minimum energy conformer structure has been optimized for the structural parameters and vibrational modes of the molecule. The FT-IR, FT-Raman and bond length values were obtained theoretically by DFT/B3LYP/6-311++G(d,p) and compared with experimental values. Charge transformation within 5TDOP was calculated using frontier molecular orbitals. The band gap energy obtained between HOMO and LUMO is 5.0740 eV which is closely related to UV-Vis value. The transition from HOMO to LUMO shows the maximum distribution of electrons. The stabilization energies are calculated in LP(O), LP(Cl) and LP(N) donors that are interacted with the neighboring anti-bonding acceptors. The second order non-linear optical effects of 5TDOP have been reported by hyperpolarizability. Furthermore, the non-zero value of the dipole moment indicates that the molecule is highly polar. The nucleophilic and electrophilic nature of the molecule has been explained by MEP and Fukui reactivity receptors. ELF and LOL highlight the chemically significant region of 5TDOP. The estimated binding energy with hydrogen bond lengths using 4B70 and 4B72 proteins have been calculated which shows that 5TDOP can act as a membrane permeable inhibitor.

Declarations

Author contribution statement

S. Sevvanthi: Conceived and designed the experiments; Performed the experiments; Analyzed and interpreted the data; Contributed reagents, materials, analysis tools or data; Wrote the paper.

S. Muthu: Conceived and designed the experiments; Contributed reagents, materials, analysis tools or data.

M. Raja: Performed the experiments; Analyzed and interpreted the data.

S. Aayisha, S. Janani: Analyzed and interpreted the data.

Funding statement

This research did not receive any specific grant from funding agencies in the public, commercial, or not-for-profit sectors.

Competing interest statement

The authors declare no conflict of interest.

Additional information

No additional information is available for this paper.

References

[1] S. Kakkar, S. Tahlan, S.M. Lim, K. Ramasamy, V. Mani, S.A. A Shah, B. Narasimhan, Benzoxazole derivatives: design, synthesis, and biological evaluation, Chem. Cent. J. 12 (1) (2018).
[2] R. Kaur, V. Rani, V. Abbot, et al., Recent synthetic and medicinal perspectives of pyrroles: an overview, J. Pharm. Chem. Chem. Sci. 1 (1) (2017) 17–32.
[3] T. Boer, E. Meulman, H. Meijering, J. Wieling, P. Dogterom, H. Lass, Quantification of asenapine and three metabolites in human plasma using liquid chromatography-tandem mass spectrometry with automated solid-phase extraction: application to a phase I clinical trial with asenapine in healthy male subjects, Biomed. Chromatogr. 26 (2) (2011) 156–165.
[4] M. Protti, A. Vignali, T. Sanchez Blanco, J. Rudge, F. Bugamelli, A. Ferranti, L. Mercolini, Enantioseparation and determination of asenapine in biological fluid micromatrices by HPLC with diode array detection, J. Sep. Sci. 41 (6) (2018) 1257–1265.
[5] N.P. Patel, M. Sanyal, N. Sharma, D.S. Patel, P.S. Shrivastav, B.N. Patel, Determination of asenapine in presence of its inactive metabolites in human plasma by LC-MS/MS, J. Pharm. Sci 8 (5) (2018) 341–347.
[6] C. Miller, O. Pleitez, D. Anderson, D. Mertens-Maxham, N. Wade, Asenapine (Saphris(R)): GC-MS method validation and the postmortem distribution of a new atypical antipsychotic medication, J. Anal. Toxicol. 37 (8) (2013) 559–564.
[7] L. Citrome, D. Walling, C. Zeni, M. Komaroff, A. Park, O50. Efficacy and safety of an asenapine transdermal patch (asenapine transdermal system, HP-3070) in the treatment of adults with schizophrenia: a phase 3, randomized, double-blind, placebo-controlled, 6-week inpatient study, Biol. Phychiatry 85 (10) (2019) S126.
[8] S.A. Karaca, D.Y. Ugur, A stability indicating ion-pair lc method for the determination of asenapine in pharmaceuticals, J. Chil. Chem. Soc. 62 (1) (2017) 3325–3329.
[9] R.R. Anugu, P.S. Mainkar, B. Sridhar, S. Chandrasekhar, The Ireland–Claisen rearrangement strategy towards the synthesis of the schizophrenia drug, (+)-asenapine, Org. Biomol. Chem. 14 (4) (2016) 1332–1337.
[10] V.M. Gambhire, Enhanced oral delivery of asenapine maleate from solid lipid nanoparticles: pharmacokinetic and brain distribution evaluations, Asian J. Pharm. 12 (3) (2018).
[11] A.D. Becke, Perspective: fifty years of density-functional theory in chemical physics, J. Chem. Phys. 140 (18) (2014) 18A301.
[12] W. Kohn, L.J. Sham, Self-consistent equations including exchange and correlation effects, APS 140 (1965) A1133–A1138.
[13] A.D. Becke, Density-functional thermochemistry. III. The role of exact exchange, Chem. Phys. 98 (7) (1993) 5648–5652.
[14] M.J. Frisch, G.W. Trucks, V.G. Zakrzewski, Ortiz, J. Cioslowski, D.J. Fox, et al., Gaussian 09, Revision E.01, Gaussian, Inc., Wallingford CT, 2009.
[15] R. Dennington, T. Keith, J. Millam, GaussView, Semichem Inc., Shawnee Mission, KS, 2009. Version 5.
[16] M.H. Jamroz, Vibrational Energy Distribution Analysis, VEDA 4 Program Warsaw, Poland, 2004.
[17] S. Aayisha, T.S. Renuga Devi, S. Janani, S. Muthu, M. Raja, S. Sevvanthi, DFT, molecular docking and experimental FT-IR, FT-Raman, NMR inquisitions on "4-chloro-N-(4,5-dihydro-1H-imidazol-2-yl)-6-methoxy-2-methylpyrimidin-5-amine": alpha-2-imidazoline receptor agonist antihypertensive agent, J. Mol. Struct. 1186 (2019) 468–481.
[18] T. Lu, F. Chen, Multiwfn: a multifunctional wavefunction analyzer, J. Comput. Chem. 33 (2012) 580–592.
[19] S. Azam, S. Abbasi, Molecular docking studies for the identification of novel melatoninergic inhibitors for acetylserotonin-O-methyltransferase using different docking routines, Theor. Biol. Med. Model. 10 (1) (2013) 63.
[20] S. Aayisha, T.S. Renuga Devi, S. Janani, S. Muthu, M. Raja, S. Sevvanthi, B.R. Raajaraman, Vibrational and computational analysis for molecular structure properties of N-(2-(trifluoromethyl)phenyl)acetamide: density functional theory approach, Spectrosc. Lett. 52 (9) (2019) 563–576.
[21] V. Karunakaran, V. Balachandran, FT-IR, FT-Raman spectra, NBO, HOMO–LUMO and thermodynamic functions of 4-chloro-3-nitrobenzaldehyde based on ab initio HF and DFT calculations, Spectrochim. Acta A 98 (2012) 229–239.
[22] Christina Susan Abraham, Johanan Christian Prasana, S. Muthu, B. Fathima Rizwana, M. Raja, Quantum computational studies, spectroscopic (FT-IR, FT-Raman and UV-Vis) profiling, natural hybrid orbital and molecular docking analysis on 2,4 Dibromoaniline, J. Mol. Struct. 1160 (2018) 393–405.
[23] K. Furie, V. Mohcek, M. Bonifacic, I. Stefanic, Raman spectroscopic study of H2O and D2O water solutions of glycine, J. Mol. Struct. 267 (1992) 39–44.
[24] S. Sevvanthi, S. Muthu, M. Raja, Quantum mechanical, spectroscopic studied and molecular docking analysis on 5,5-diphenylimidazolidine-2,4-dione, J. Mol. Struct. 1149 (2017) 487–498.
[25] A. Prabakaran, S. Muthu, Normal coordinate analysis and vibrational spectroscopy (FTIR and FT-Raman) studies of (S)-2-amino-3-(3,4-dihydroxyphenyl)-2-methylpropanonic acid using ab initio HF and DFT method, Spectrochim. Acta A 99 (2012) 90–96.
[26] G. Varsanyi, Assignment for Vibrational Spectra of Seven Hundred Benzene Derivatives, Academic Kiaclo, Budapest, 1973.
[27] J. Mohan, Organic Spectroscopy Principles and Aplications, Narosa Publishimg House, New Delhi, 2001.
[28] S. Gunasekaran, S. Kumaresan, R. Arunbalaji, G. Anand, S. Seshadri, S. Muthu, Vibrational assignments and electronic structure calculations for 6-thioguanine, J. Raman Spectrosc. 40 (2019) 1675–1681.
[29] A.J. Barnes, M.A. Majid, M.A. Stuckey, P. Gregory, C.V. Stead, Quantum mechanicl study and spectroscopic (FT-IR, FT-Raman, ^{13}C, ^{1}H, UV) study, first order hyperpolarizability, NBO analysis, HOMO and LUMO analysis of 4-[(4-aminobenzene) sulfonyl]aniline by ab initio HF and density functional method, Spectrochim. Acta A 4 (1985) 629–635.
[30] T. Rajamani, S. Muthu, M. Karabacak, Electronic absorption, vibrational spectra, nonlinear optical properties, NBO analysis and thermodynamic properties of N-(4-nitro-2-phenoxyphenyl) methanesulfonamide molecule by ab initio HF and density functional methods, Spectrochim. Acta A 108 (2013) 186–196.
[31] M. Karabacak, C. karaka, A. Atac, M. Eskici, A. Karanfil, Synthesis, analysis of spectroscopic and nonlinear optical properties of the novel compound: (S)-N-benzyl-1-phenyl-5-(thiophen-3-yl)-4-pentyn-2-amine, Spectrochim. Acta A 97 (2012) 556–567.
[32] S. Gunasekaran, U. Ponnambalam, S. Muthu, S. Ponnusamy, Vibrational and normal coordinate analysis of pyrazinamide, Asian J. Chem. 16 (23) (2004) 1513–1518.
[33] S. George, Infrared and Raman Characteristic Group Frequencies, Tables and Charts, third ed., Wiley, New York, 2001.
[34] C.H. Kaschula, T.J. Egan, R. Hunter, N. Basilico, S. Parapini, D. Taramelli, E. Pasini, D. Monti, Structure– activity relationships in 4-aminoquinoline antiplasmodials. The role of the group at the 7-position, J. Med. Chem. 45 (16) (2002) 3531–3539.

[35] N. Muruganantham, R. Sivakumar, N. Anbalagan, V. Gunasekaran, J.T. Leonard, Synthesis, anticonvulsant and antihypertensive activities of 8-substituted quinoline derivatives, Biol. Pharm. Bull. 27 (10) (2004) 1683–1687.
[36] S. Sevvanthi, S. Muthu, M. Raja, Molecular docking, vibrational spectroscopy studies of (RS)-2-(tert-Butylamino)-1-(3-chlorophenyl)propan-1-one: a potential Adrenaline uptake inhibitor, J. Mol. Struct. 1173 (2018) 251.
[37] M. Raja, R. Raj Muhamed, S. Muthu, M. Suresh, Synthesis, spectroscopic (FT-IR, FT-Raman, NMR, UV–Visible), NLO, NBO, HOMO-LUMO, Fukui function and molecular docking study of (E)-1-(5-bromo-2-hydroxybenzylidene)semicarbazide, J. Mol. Struct. 1141 (2017) 284–298.
[38] S. Muthu, J. Uma Maheswari, Quantum mechanical study and spectroscopic (FT-IR, FT-Raman, 13C, 1H, UV) study, first order hyperpolarizability, NBO analysis, HOMO and LUMO analysis of 4-[(4-aminobenzene) sulfonyl] aniline by ab initio HF and density functional method, Spectrochim. Acta A 92 (2012) 154–163.
[39] N. Swarnalatha, S. Gunasekaran, S. Muthu, M. Nagarajan, Molecular structure analysis and spectroscopic characterization of 9-methoxy-2H-furo[3,2-g]chromen-2-one with experimental (FT-IR and FT-Raman) techniques and quantum chemical calculations, Spectrochim. Acta A 137 (2015) 721–729.
[40] L.S. Anju, D. Aruldhas, I. Hubert Joe, S. Balachandran, Density functional theory, spectroscopic and hydrogen bonding analysis of fenoxycarb–water complexes, J. Mol. Struct. 1201 (2019) 127201.
[41] C. Morell, A. Grand, A. Toro-Labbé, New dual descriptor for chemical reactivity, J. Phys. Chem. A 109 (1) (2005) 205–212.
[42] B.F. Rizwana, S. Muthu, J.C. Prasana, C.S. Abraham, M. Raja, Spectroscopic (FT-IR, FT-Raman) investigation, topology (esp, elf, lol) analyses, charge transfer excitation and molecular docking (dengue, hcv) studies on ribavirin, Chem. Data Collections 17–18 (2018) 236–250.
[43] M. Raja, R.R. Muhamed, S. Muthu, M. Suresh, Synthesis, spectroscopic (FT-IR, FT-Raman, NMR, UV–Visible), first order hyperpolarizability, NBO and molecular docking study of (E)-1-(4-bromobenzylidene)semicarbazide, J. Mol. Struct. 1128 (2017) 481–492.
[44] D.V. Fernando, A.S. David, T. Yoshinari, A. Xavier, R. Angel, G.L. Steven, J.R. John, Basis set effects on the hyperpolarizability of CHCl_3: Gaussian-type orbitals, numerical basis sets and real-space grids, J. Chem. Phys. 133 (2010), 034111.
[45] J.R.A. Silva, J. Lameira, C.N. Alves, Insights for design of Tripanosoma cruzi GAPDH inhibitors: a QM/MM MD of 1,3-bisphospho-D-glyceric acid analogs, Int. J. Quant. Chem. 112 (2012) 3398–3402.
[46] P. Ramesh, M. Lydia Caroline, S. Muthu, B. Narayana, M. Raja, S. Aayisha, Spectroscopic and DFT studies, Structural determination, Chemical properties and Molecular docking of 1-(3-Bromo-2-thienyl)-3-[4-(dimethylamino)-phenyl]prop-2-en-1-one, J. Mol. Struct. 1200 (2019) 127123.
[47] X. Liang, J. Jiang, X. Xue, L. Huang, X. Ding, D. Nong, Synthesis, characterization, photoluminescence, anti-tumor activity, DFT calculations and molecular docking with proteins of zinc(ii) halogen substituted terpyridine compounds, Dalton Trans. 48 (28) (2019) 10488–10504.